AIAA Atmospheric Flight Mechanics Conference
10 - 13 August 2009, Chicago, Illinois

AIAA 2009-6154

A Model-Based Approach to Aircraft Takeoff and Landing Performance Assessment

P. Ohme*

DLR, German Aerospace Center

Institute of Flight Systems

Lilienthalplatz 7, 38108 Braunschweig, Germany

This paper reports a newly developed software tool, called MAPET II, for evaluation of aircraft takeoff and landing performance based on a 6-DOF high fidelity model. It describes the succeeding work of the development of MAPET for climb, descent and cruise performance assessment presented in a previous AIAA paper.[1] Takeoff performance is, according to FAR 25, defined by the covered distances and reference speeds during the takeoff run. MAPET II allows to determine these for aircraft certification important parameters from a simulation model automatically. Basic conditions like aircraft weight, CG position, flaps setting or the runway elevation can be defined over a graphical user interface. Another feature is the determination of landing distances. The most important parameters for landing like aircraft mass, approach speed and runway condition (dry, wet, icy) can be varied as well. Furthermore, it is possible to study the effects of failure cases like the loss of reverse thrust, spoilers or landing gear brakes. The results are presented for a generic future military transport aircraft model, but the modular structure of MAPET II allows the integration of every flight mechanical simulation model with similar model structure.

Nomenclature

α	Angle of attack, [°]
α_{stall}	Stall angle of attack, [°]
β	Sideslip angle, [°]
γ	Flight path angle, [°]
Φ	Roll angle, [°]
Ψ	Yaw angle, [°]
Θ	Pitch angle, [°]
A/C	Aircraft
C_L	Total lift coefficient , [-]
CG	Center of gravity position of the aircraft, [% MAC]
FAA	Federal Aviation Authority
FAR	Federal Aviation Regulations
FMTA	Future Military Transport Aircraft
FP	Flight path
GUI	Graphical User Interface
MAPET	Model based Aircraft Performance Evaluation Tool
MiTraPor	Military Transport Aircraft
MLG	Main landing gear
NG	Nose gear
Rev	Reverser
RW	Runway

*Project Research Scientist, per.ohme@dlr.de

Copyright © 2009 by P. Ohme, DLR. Published by the American Institute of Aeronautics and Astronautics, Inc., with permission.

SB	Speed brakes
TOD	Takeoff distance
V_1	Takeoff decision speed, [kt]
V_2	Takeoff safety speed, [kt]
V_{EF}	Engine failure speed, [kt]
V_{ELV}	Speed at initiation of rotation (Begin of elevator deflection), [kt]
V_{IAS}	Indicated airspeed, [kt]
V_{LOF}	Liftoff speed, [kt]
$V_{MCA-dyn}$	Minimum Control Speed Air (dynamic test), [kt]
$V_{MCA-stat}$	Minimum Control Speed Air (static test), [kt]
V_{MCA}	Minimum Control Speed Air, [kt]
V_{MCG}	Minimum Control Speed Ground, [kt]
V_{MU}	Minimum Unstick Speed, [kt]
V_R	Rotation speed, [kt]
V_S	Stall speed, [kt]

I. Introduction

Already in the early phase of an aircraft design process takeoff and landing performance are of essential importance. Basic design parameters like the aircraft mass, wing surface area, stabilizer position, size of the control surfaces etc. are derived from the flight tasks which always include takeoff and landing. For these flight phases certain requirements concerning the required runway lengths have to be fulfilled. In addition different speeds have to be considered for the takeoff phase. These speeds are defined in the FAR 25[4] and their determination and verification is an important component for the certification of an airplane. For this purpose, normally an extensive flight test program is carried out.

A software tool MAPET II presented in this paper was developed for the model-based determination of takeoff and landing performance and is a follow-up development of MAPET, a software tool to determine climb, descent and cruise flight performance.[1] Both tools were developed within the DLR research project 'MiTraPor'. Among others, the aim of 'MiTraPor' is to extend the evaluation capability of modern military transport aircrafts. Hence, a detailed flight-mechanical 6 DOF simulation model of such an aircraft (FMTA) was developed. This model is used for all evaluations presented in this paper. MAPET II allows as well as MAPET through its modular structure a simple and quick implementation of other similar structured aircraft models.

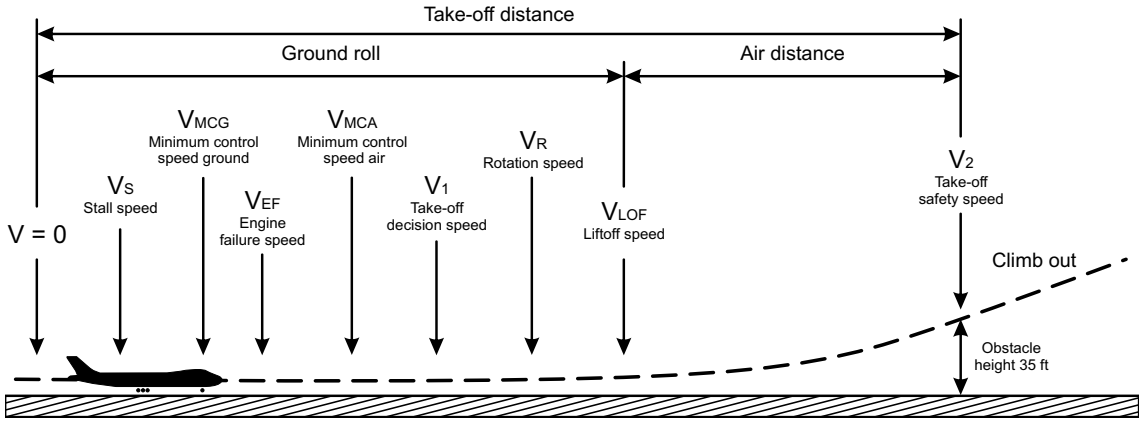

Figure 1. Takeoff distances and reference speeds (FAR 25)

Takeoff performance is defined in general by the covered distances on the runway and the reference speeds during the takeoff according to FAR 25. Figure 1 shows the definitions of the takeoff distances and reference speeds for the typical sequences of a takeoff trajectory.

MAPET II allows a very quick determination of all the speeds indicated by Figure 1 using a simulation model. The concept of this model-based approach is explained in detail in chapter II. Important parameters like aircraft mass, CG position, flaps position or runway elevation are definable by a graphical user interface. More details on the determination process for a respective takeoff reference speed are given in chapter III.

Another feature of MAPET II is the simulation-based determination of landing distances. As a substitute for manual pilot inputs a controller was implemented to automate the landing procedure. A detailed description of the landing scenario gives chapter IV. Figure 2 shows the definitions of the landing distances according to FAR 25. Influencing variables like aircraft mass, approach speed or the runway condition (dry, wet, icy) can be varied again by the graphical user interface. Additionally it is possible to study the effects of failure cases like a loss of thrust reverse or spoilers.

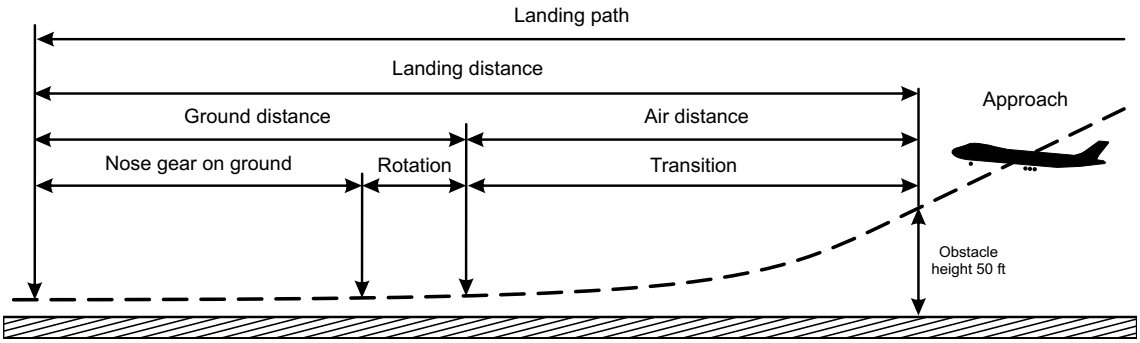

Figure 2. Landing distances (FAR 25)

II. Concept of the software tool MAPET II

The concept of MAPET, the software tool for model-based assessment of climb, descent and cruise performance presented in Ref. 1 is based on trim calculations of steady aircraft states for predefined aircraft mass, altitude and speed ranges. This concept could not be applied here because takeoff and landing consist of dynamic acceleration and deceleration processes. Hence, the idea was to determine takeoff and landing performance directly from the simulations. Instead of performing flight tests with pilots in the simulator the MATLAB/Simulink®based software tool MAPET II was developed to derive all important performance parameters from standardized simulations automatically. According to the instructions of the 'FAA Advisory Circular'[4] for determination of the takeoff reference speeds and the landing distances (see chapter I) for every task an own test scenario was developed. The control inputs for each test are generated by logically linked switches (e.g. beginning of takeoff thrust, thrust reverse, gear brake etc.) and controllers for rudder, ailerons or thrust. Stall speed V_S and the static 'Minimum Control Speed Air' V_{MCA}-static were determined by trim calculations of steady flight states.

Figure 3 shows the basic concept and structure of MAPET II. The MAPET II computation processes are managed by the main program. It immediately launches the graphical user interface for the definition of the input parameters like aircraft mass, flaps setting, CG position, runway elevation etc. The execution of the simulation and finally the evaluation of the simulation results can be controlled for every test scenario. All together 8 automated test scenarios are implemented using the centrally stored 6 DOF aircraft model.

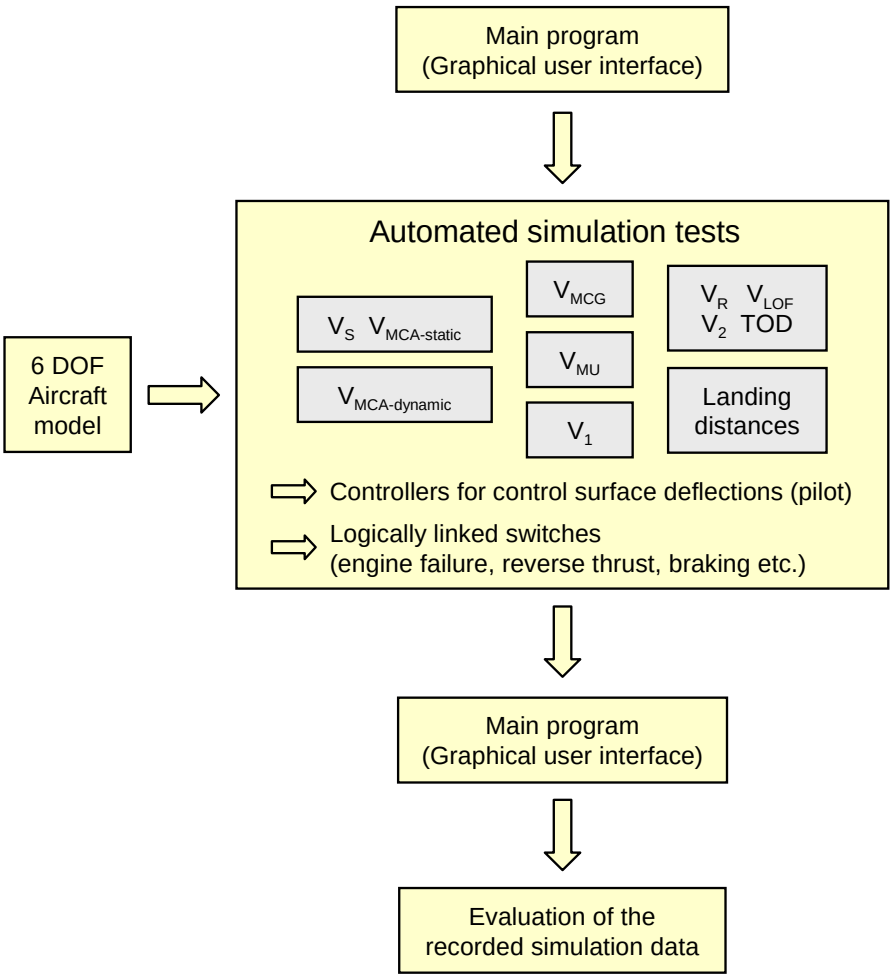

Figure 3. Concept for the model-based determination of takeoff and landing performance

III. Takeoff Performance

A. Rotation speed V_R, Liftoff speed V_{LOF} and Takeoff safety speed V_2

The 'Rotation Speed' V_R defines the speed during the takeoff process at which the aircraft begins to rotate, i.e. the nose gear lifts off from ground. When reaching the 'Liftoff Speed' V_{LOF} the main landing gear lifts off from ground so that the aircraft is airborne beyond that point. V_2 identifies the speed at which the aircraft reaches the obstacle height of 35 ft. According to FAR 25 it is required to hold a minimum specified climb gradient up to 400 ft height at V_2 with one-engine inoperative. For a 4-engine aircraft this climb gradient is 3%, i.e. a flight path angle of approximately 1.7°. Defining a simulation test to determine V_R, V_{LOF} and V_2 without previous knowledge about the aircraft characteristics may be complicated because the takeoff procedure is influenced by individual pilot techniques and behaviors. In order to get a flight physical evaluation as objective as possible the pilots individual influence is not considered for this test and a controller for elevator deflection is implemented to perform the takeoff task as effective as possible. The most important variable parameter during takeoff phase is the speed at which the rotation is initiated (here defined as V_{ELV}), i.e. pulling the stick to deflect the elevator. Directly dependent on this speed are V_R shortly after, V_{LOF} and V_2 in the following takeoff run. The aim of this approach is the determination of V_{ELV} (V_R) which minimizes the takeoff distance. The takeoff test under varying V_{ELV} is executed in a program loop as explained in the following: At first a trimming calculation of a steady climb at the obstacle height of 35 ft, takeoff thrust and a pitch angle of 20° is performed. The pitch angle of 20° was defined as the target angle for climb after the aircraft has passed the obstacle height. This calculation is only conducted to

determine the correct trimming position for the horizontal stabilizer in advance to know the target elevator deflection at the 35 ft height. In this condition the aircraft is placed on the runway. After a short damper compression of the landing gear the thrust levers are switched to takeoff position and the aircraft begins to accelerate. When reaching V_{ELV} which is varied every takeoff run a controller for the elevator deflection provides at first a pitch angle of 13°. The geometrical limitation at which the aircraft tail touches the ground is 14.8°. After liftoff the target pitch angle for the controller is slowly increased to 20°. At the obstacle height of 35 ft when the takeoff safety speed V_2 is reached the simulation is stopped.

As an example three diagrams in Figure 4(a) show altitude (aircraft CG), pitch angle Θ and speed (V_{IAS}) versus the covered distance on the runway for three different takeoff runs at maximum takeoff weight of 130 t. The sequence of the takeoff run at which the aircraft rotates and lifts off is zoomed out. In test case 1 the rotation is initiated at the speed of V_{ELV} = 132 kt, in case 2 at 134 kt and in case 3 at 146 kt. The circles indicate the nose gear liftoff, the crosses show the main landing gear liftoff. The black dashed line in the Θ-diagram marks the geometrical limitation (tail on ground) of the aircraft which is only relevant for the part of the takeoff run at which the main landing gear is on ground. The initiation of the rotation in takeoff case 1 is too soon. Keeping the limitation of the maximum pitch attitude before liftoff the speed is not high enough that the aircraft is able to produce as much lift force as required for liftoff. The aircraft rotates up to 13° pitch angle and accelerates without lifting off. This aircraft state produces unnecessary more drag at an earlier stage than in takeoff case 2. For this reason the speed at the same covered distance is in case 1 a little lower (approx. 0.5 kt) than in case 2 so that liftoff is still not possible. During the pitch-up phase on ground in case 1 the controller tries to hold the target pitch angle being only possible with some variations. Because of this the liftoff speed in test case 1 is about 8 kt higher than in test case 2. The initiation of the rotation in test case 3 occurs too late. The higher speed produces a higher dynamic pressure with a corresponding increase of elevator effectiveness compared to test cases 1 and 2. For this reason the rotation process until liftoff is faster but the distance covered on the runway is already too high at that point.

Figure 4(b) shows the covered takeoff distance at V_{LOF} versus rotation speed V_R for 32 takeoff cases with different speeds for initiation of the rotation phase (V_{ELV}). This evaluation is performed for 3 different initial conditions, for maximum takeoff weight of 130 t and airfield elevations of 0 ft (red curve) and 8000 ft (black curve) and for 90 t aircraft mass and an airfield elevation of 0 ft (blue curve). The three takeoff cases shown in the upper diagrams are marked through the numbers 1, 2 and 3 in the corresponding red curve. It is evident that every curve has a distinctive minimum, i.e. there is an optimum rotation speed to minimize the takeoff distance. The optimum test case 2 on the red curve has a takeoff distance at V_{LOF} of 3796 ft for a speed to initiate the rotation of V_{ELV} = 134 kt and the rotation speed of V_R = 137 kt. The takeoff tests for the same aircraft mass but at an airfield elevation of 8000 ft show generally longer takeoff distances. This is because of the lower air density so that the engine power decreases and a higher flow velocity is required to generate equivalent aerodynamic forces. The indicated airspeed at 8000 ft is only a little higher than in the test case at 0 ft airfield elevation however the true airspeeds being relevant for the development of the aerodynamic forces are much higher. The minimum takeoff distance in this case is 5256 ft at V_{ELV} = 136 kt and V_R = 138 kt. As expected the takeoff tests at sea level with an aircraft mass of 100 t (blue curve) show generally shorter takeoff distances than the tests with maximum takeoff weight at sea level. This yields smaller values for V_{ELV} = 115 kt and for V_R = 117 kt as well because the aircraft requires less lift force for taking off. Additionally the curves in Figure 4(b) give approximate values for the speed at which the elevator effectiveness is sufficient to initiate the rotation. Below a certain speed there is nearly no effect deflecting the elevator (for longitudinal motion equivalent to the V_{MCG}-test for lateral motion, see chapter III B). For 130 t aircraft mass this minimum V_R is approximately 103 kt and for 80 t it is about 95 kt.

Concerning these evaluations it has generally to be pointed out that the shape and to some degree the position of the TOD-minima are dependent on the controller settings. All takeoff tests were performed using the same controller settings. Since the aircraft characteristics have changed through variation of aircraft mass and runway elevation the shapes of the curves minima show different profiles. In all cases the generated elevator deflections could also be carried out by a human pilot. The essential characteristic of the curves to form a minimum is independent on reasonable controller settings. The position of the minima shifts only by a few knots so that the optimum values for V_R and V_{LOF} determined here can be regarded as realistic.

If this variation is comparable to the variation caused by different test pilots in a flight test program to evaluate the optimum V_R is subject of future work to find the most realistic controller concept, pilot model etc.

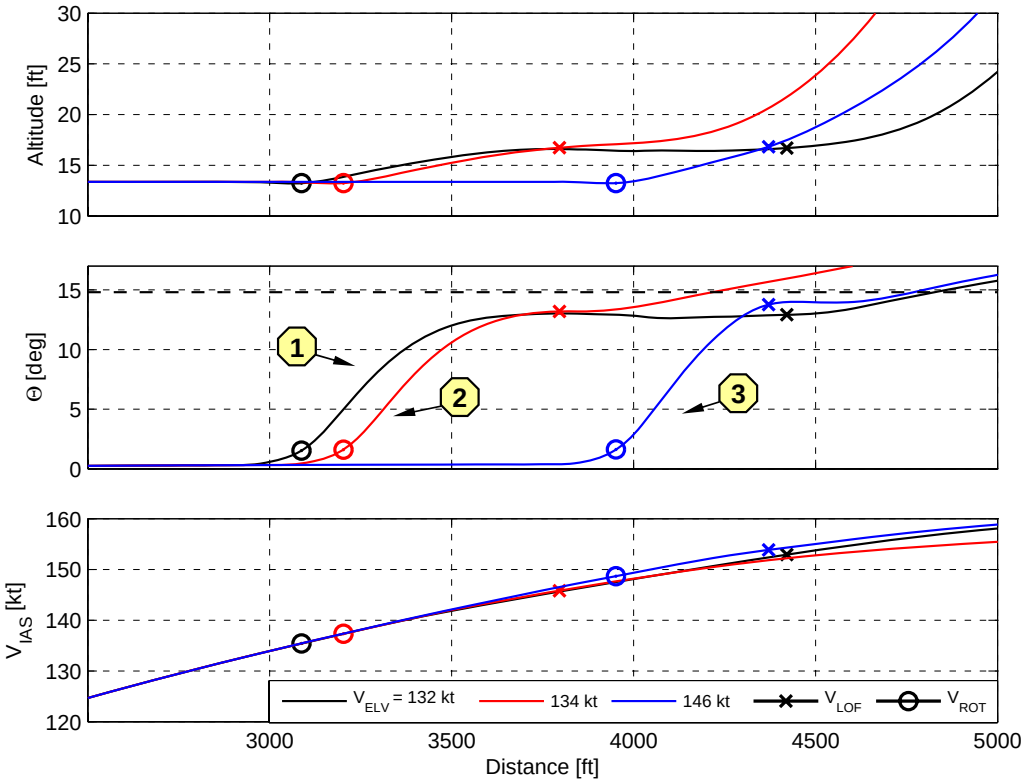

(a) Three takeoff examples

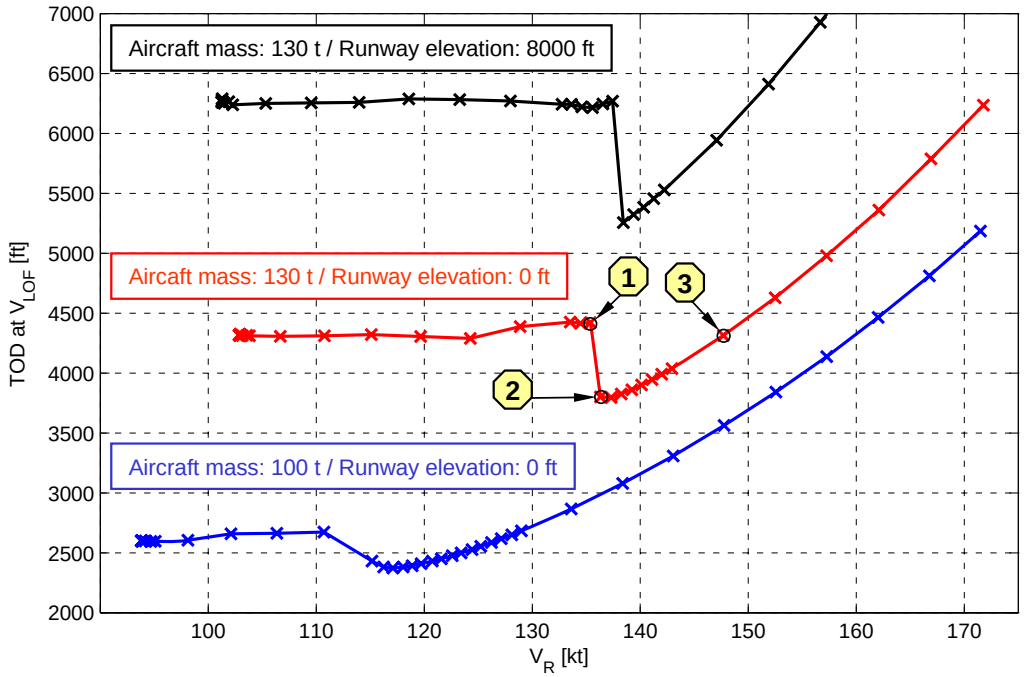

(b) Takeoffs under different conditions

Figure 4. Evaluation of V_R and V_{LOF}

Figure 5 shows once more the curve to determine V_R, V_{LOF} and V_2 for an aircraft mass of 130 t at sea level (see red curve Fig. 4(a)), but now all numerical values for the optimum takeoff case are listed. The displayed safety speed V_2 takes place when reaching the obstacle height of 35 ft. To fulfill the FAR 25 criteria for V_2 an additional trim calculation in the post processing is performed to check whether V_2 can be kept with one engine inoperative and a minimum flight path angle of 1.7° at 400 ft altitude. The trim calculation of a steady climb is carried out with retracted landing gear, takeoff flaps setting, takeoff thrust and the left outer engine inoperative. Figure 5 shows the results under 'V_2 check'. The resulting flight path angle here is 3.1° (i.e. greater than 1.7 °) confirming a V_2 of 156 kt determined in this test.

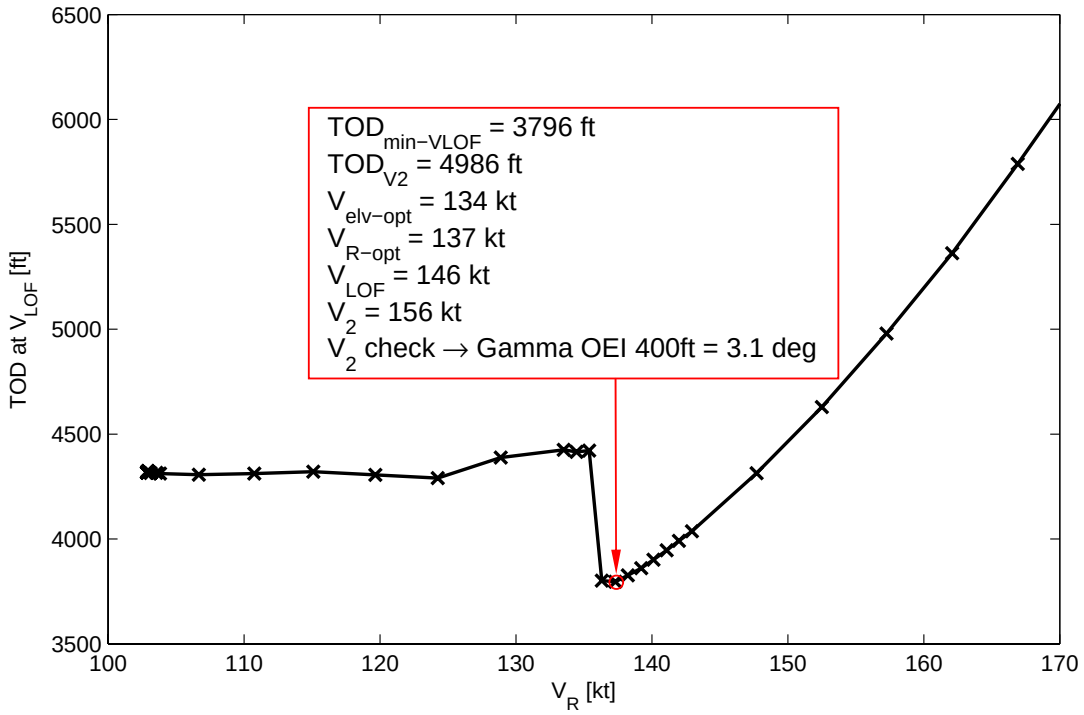

Figure 5. Plot of results for V_R, V_{LOF} and V_2 evaluation

The diagrams in Figure 6 show the result if the above explained evaluations are carried out for different aircraft masses. The upper diagram shows the takeoff distance at V_{LOF} versus aircraft mass for two different runway elevations. In both cases an increase of takeoff distance for increasing aircraft mass can be recognized and because of the reasons mentioned before the takeoff distances are generally longer at 5000 ft. The lower diagram shows the rotation speed versus aircraft mass of both takeoff runway elevations. An increase of V_R for increasing aircraft masses can be seen here as well.

The generation of these diagrams requires the highest computational effort. For each point displayed here a TOD minimum determination like illustrated in Figure 5 is required. For each minimum TOD calculation 30 to 40 simulations of the takeoff process are necessary, all together up to 720 simulations are performed to produce the curves of Figure 6. Additionally for every runway elevation and aircraft mass one trim calculation to determine the initial horizontal stabilizer position and one trim calculation for the 'V_2 check' are necessary.

B. Minimum control speed ground V_{MCG}

'Minimum Control Speed Ground' V_{MCG} defines the speed during the ground roll phase of a takeoff process from which the aircraft can be held on the runway and therefore remains controllable after an engine failure only using rudder deflection. In that case the aerodynamic side force of the full deflected rudder is sufficient to compensate the moment originating from the asymmetrical thrust caused by the engine failure.

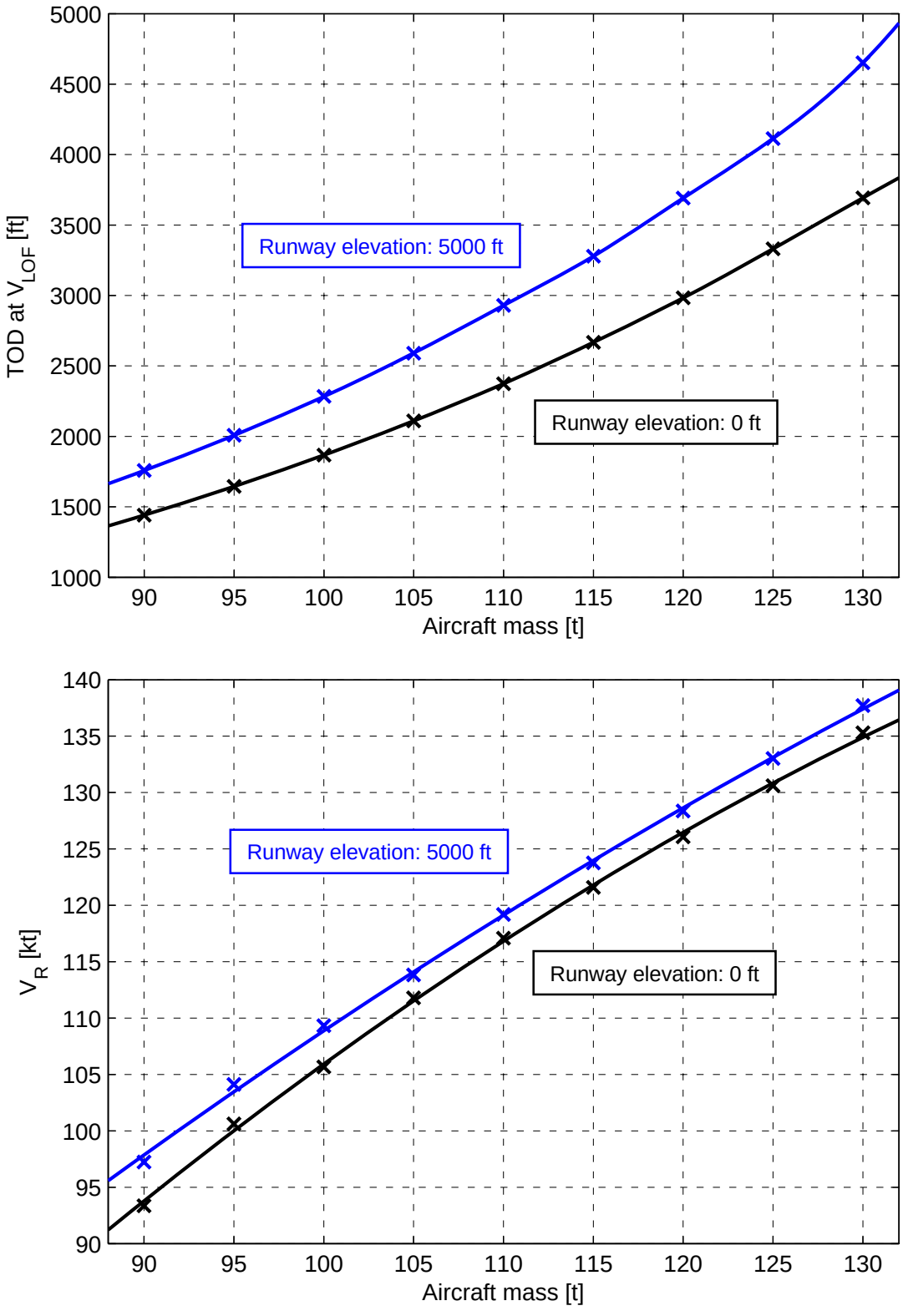

Figure 6. Takeoff distance at V_{LOF} and V_R versus aircraft mass

For certification according to FAR 25 it must be proven by takeoff tests that the aircraft deviation from the runway center line is below 30 ft during ground roll for an engine failure speed ($\rightarrow V_{MCG}$).

For determination of V_{MCG} the following test scenario is implemented for the simulation: The aircraft is placed on the runway in standstill position. The thrust levers are switched to takeoff position and the aircraft begins to accelerate. At a defined speed V_{EF} the left outer engine is switched off and a rudder controller provides the minimization of the deviation of the aircraft center of gravity from the runway center line. The three remaining engines maintain takeoff thrust. If the aircraft regains the runway center line the simulation is stopped. Now the aim is to determine that speed by variation of V_{EF} at which the deviation from the center line is 30 ft ($\rightarrow V_{MCG}$). At first 4 simulations with predefined V_{EF} (78, 117, 156, 175 kt) are executed automatically. The choice of these speeds make sure that V_{MCG} is within this covered range. The maximum deviation from the runway center line for each V_{EF} simulation trial is used as an optimization criterion to approach the target value of 30 ft iteratively. Finally, if the maximum deviation from runway center line meets the termination criterion the iteration process of simulations is stopped and the V_{MCG} providing a maximum deviation of 30 ft is found.

Figure 7 illustrates the result of such an iteration process. The diagram shows the deviation of the aircraft CG position from the runway center line versus the covered distance. The solid curves in black, green, red and blue show the takeoff cases at the predefined engine failure speeds. The points of the engine failure are marked through circles on the respective curves. For the first both runs the rudder effectiveness is not sufficient to keep the deviation below 30 ft, for the last both runs the deviation is below 30 ft. The black dashed curve shows the final result of the iteration, thus V_{MCG} of 130 kt is determined.

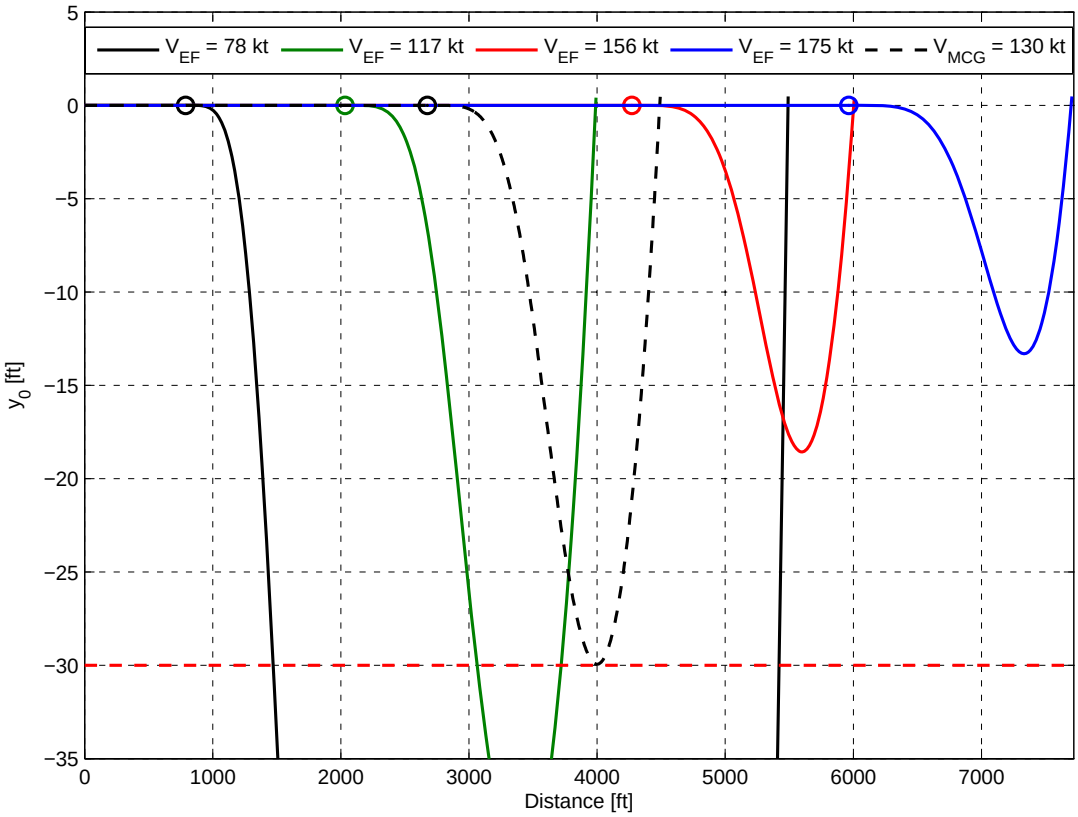

Figure 7. Determination of V_{MCG} for an aircraft mass of 125 t at sea level

C. Takeoff decision speed V_1

V_1 defines the speed during a takeoff beyond which the pilot has to continue the takeoff after an engine failure. If the engine failure occurs before V_1 the remaining runway section is long enough to abort the takeoff and to stop the aircraft before the end of the runway. Thus, it is quite clear that the main influence parameters for V_1 are the aircraft mass, the available runway length and the effectiveness of the braking systems. To consider the response time of the pilot the period from engine failure to the initiation of all braking procedures is assumed 3 seconds according to FAR 25. V_1 is precisely defined to be the speed one second after engine failure.

The determination of V_1 using simulations is carried out by the following automated test scenario: The aircraft is put on the runway in standstill position. The thrust levers are switched to takeoff position and the aircraft begins to accelerate. At a predefined speed V_{EF} the left outer engine is switched off. 3 seconds later the 3 remaining engines are shifted down into idle, the spoilers are deflected and a full braking is initiated. By means of rudder control the deviation of the aircraft from the runway center line is held as low as possible (see V_{MCG} test, subsection B). For speeds below 40 m/s this is assisted by the nose gear steering. When the aircraft has reached its standstill position, the simulation is stopped. Now the aim is to determine that engine failure speed for this test scenario at which the aircraft reaches standstill at a predefined runway length. At first 4 simulations at engine failure speeds of 78, 117, 156 and 165 kt are executed similar to the strategy for V_{MCG} determination. The choice of these speeds assure that V_1 is within the covered speed range. Using the accelerate stop distances from these simulations the engine failure speed V_{EF} at which the predefined runway length is reached is determined iteratively by additional simulations. Finally, one second after determined V_{EF} the takeoff decision speed V_1 is defined.

Figure 8 shows exemplarily such an analysis of acceleration-deceleration phases for two different aircraft masses (100 t in the upper part, 130 t below). Both diagrams show indicated airspeed versus covered distance on the runway. The maximum runway length here is 6500 ft which is marked by a red dashed line. The black, green, red and blue solid lines show the takeoff cases with V_{EF} = 78/117/156/165 kt. The circles on each curve indicate the point of engine failure and the crosses specify the point at which all above mentioned actions are initiated to decelerate the aircraft. A reduction of the acceleration between engine failure and braking is evident. On the one hand this is caused by the loss of thrust and on the other hand by the additional drag which the failed engine generates. For the same engine failure speeds the start stop distances for an aircraft mass of 100 t are generally shorter than for the aircraft mass of 130 t, because the acceleration as well as deceleration phase runs faster. This leads to a higher V_1 for the lighter aircraft. The black dashed curves show the acceleration-stop cases after the iteration for which the aircraft reaches the standstill position exactly at 6500 ft. For an aircraft mass of 100 t V_{EF} is 159 kt, for 130 t it is 147 kt. One second later V_1 can be determined being 160.7 or 148.4 kt marked through triangles.

D. Minimum control speed air V_{MCA}

The 'Minimum Control Speed Air' defines the minimum required airspeed to control a flying aircraft suffering an engine failure after takeoff. According to FAR 25 the bank angle must not exceed 5° and heading corrections must not exceed 20° to establish a steady flight state. The flaps are in takeoff position and the engine opposite the failed engine should supply full thrust. For a four engine aircraft the failure of an outer engine is required. This worst case asymmetrical thrust condition provides the most difficult situation to be controlled. The thrust of both internal engines can be used without restrictions but with symmetrical thrust. The limiting factors for the flight with asymmetrical thrust are the maximum deflections for rudder and aileron. Moreover, the maximum angle of attack α_{stall} may not be exceeded. To cover the worst case of the highest MCA speeds, the flight tests are usually performed with minimum aircraft weight.

V_{MCA} is proven by 2 different tests, a 'static test' and a 'dynamic test'. In the static test the bank angle requirement, in the dynamic test the heading deviation requirement is proved. Since the dynamic test is based on the static test, at first the static test is explained in the following.

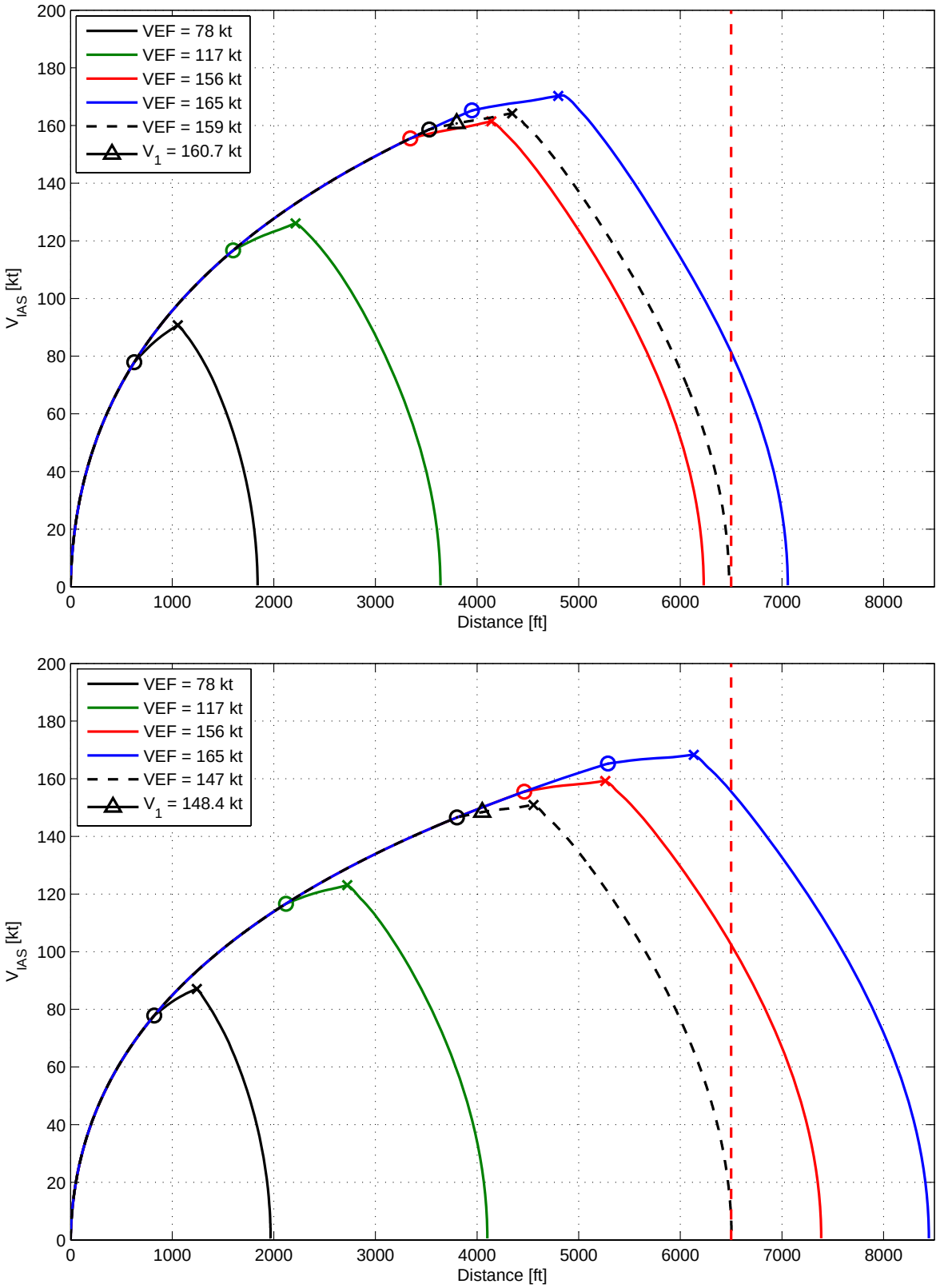

Figure 8. Determination of V_1 - A/C mass: 100 t (upper) and 130 t (lower) at sea level - RW length: 6500 ft

Static test

V_{MCA}-static is determined by flight test. The aircraft with one engine inoperative is trimmed for steady level flight (4 engine aircraft). Then the speed is continuously reduced until rudder or aileron reaches maximum deflection while the bank angle must not exceed 5°. Below this speed straight level flight cannot be performed. The test scenario for the automated determination of V_{MCA} from simulation consists of multiple trim calculations for steady flight states executed one after another. The left outer engine is shut down and the right outer engine operates with full thrust. The maximum bank angle of 5° is introduced as trim requirement. The control surface deflections and thrust lever settings of the inner engines result from the trim calculations. The initial airspeed to be trimmed is selected to be 60 m/s. Then at first it is checked whether the control surface deflections are within defined ranges (Rudder: -5° to -30° max / Ailerons: 0° to -20° max). If this is not the case more trim calculations for varying airspeeds are carried out to find a suitable initial value. In the following the speed is varied in steps of $\Delta V = +/-1$ m/s to cover the full range of rudder or aileron deflection (depending on which control surface reaches its limit first). V_{MCA}-static is obtained for the lowest speed at maximum deflection of rudder or aileron (-30° / -20°), under the condition that the maximum angle of attack α_{stall} is not exceeded.

Figure 9 illustrates the results of such an analysis for the minimum FMTA-mass of 80 t. The diagrams show angle of attack α, angle of sideslip β, rudder, aileron deflection and thrust lever setting of both inner engines versus airspeed. The ranges between the single trim points were interpolated. The red dashed lines in the aileron, rudder and thrust diagram indicate the maximum possible deflections. In this example the limiting factor for a steady level flight is the rudder deflection. The maximum of -30° is reached at an airspeed of 99.6 kt (see legend). The aileron deflection is about -12° and the angle of attack is 13°.

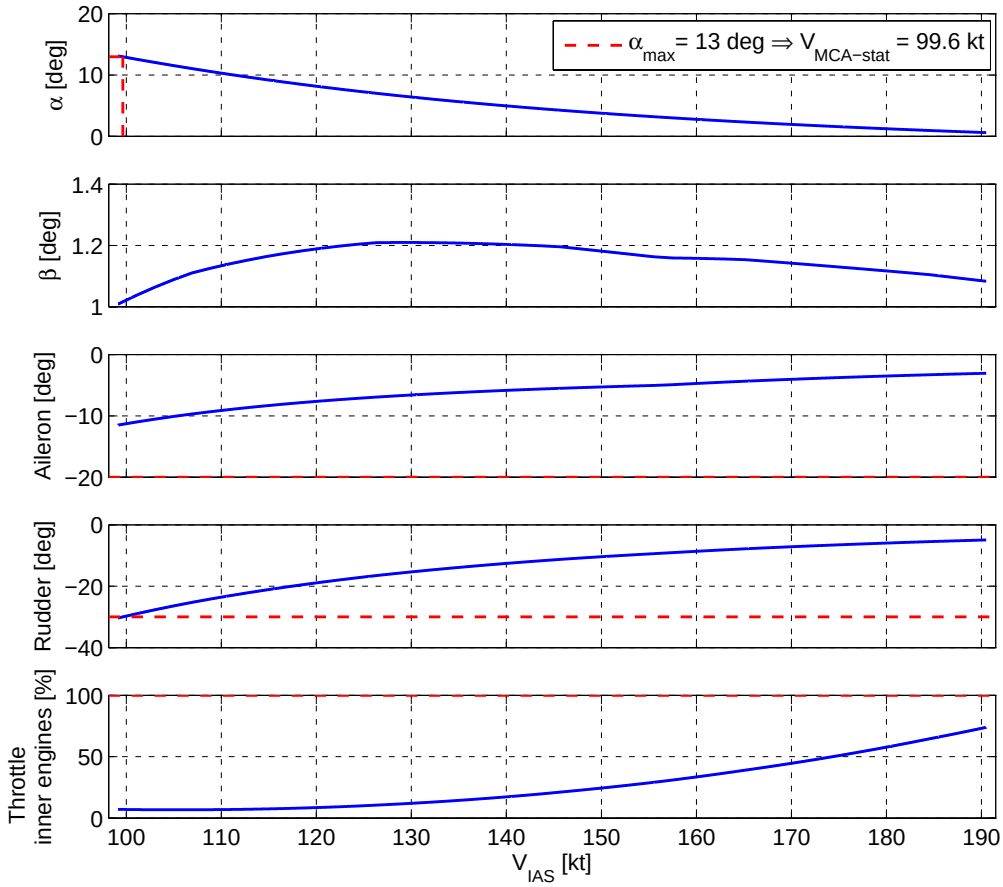

Figure 9. Determination or $V_{MCA-stat}$ for aircraft mass of 80 t and takeoff flaps setting (Static test)

It was found out by detailed investigations of V_{MCA}-static that at least for the FMTA model used in this study the lowest mass does not lead to the highest V_{MCA} (demanded according to FAR 25) like for most other aircraft designs. Figure 10 shows the analysis for maximum takeoff weight of 130 t. The red dashed lines in the upper α versus V_{IAS} diagram represents the stall angle of attack of 18°. The stall angle of attack is already reached before a control surface deflection occurs. For this example the stall speed is the relevant limitation for V_{MCA} determination. The corresponding value is 103 kt which is slightly higher than V_{MCA} for the lowest aircraft mass (see Fig. 9). Furthermore Figure 10 shows that for high aircraft masses the deflection limitation of the ailerons than those of the rudder is decisive. The reason are higher angles of sideslip for high masses (at 80 t: 1° - 1.2°, at 130 t: 4° - 8°). This results into bigger rolling moments which have to be compensated by the ailerons which are the primary controls for the roll axis. A more detailed investigation of these relations leads finally to the diagram in Figure 11. It shows $V_{MCA-stat}$ versus aircraft mass. The black curve shows the minimum airspeeds at which the surface deflections become limiting factor. At aircraft masses of 80 t to 104 t the maximum rudder deflection limits a further speed reduction, while at aircraft masses of 104 t to 130 t the ailerons are maximum deflected. The minimum of the curve represents the most efficient flight state for which both control surfaces are fully deflected, i.e. at 104 t the aircraft is controllable in level flight at the lowest $V_{MCA-stat}$ of approx. 93.5 kt. For aircraft masses greater than 106 t stall is the relevant limit. This is a rather unusual characteristic and characterizes especially the FMTA model. For most other conventional aircraft designs the stall limit lies below the control surface limits and the highest for the FAR 25 certification relevant V_{MCA} belongs to the lowest aircraft mass. Further analysis of this problem shows that the total CG position of the aircraft has considerable influence on the determination of V_{MCA}-static. For the results shown here a mid CG position was defined. Even for the FMTA aircraft model the determination of V_{MCA}-static ($\rightarrow$ highest V_{MCA}) should be conducted at lowest aircraft mass and the stall limit is below the control surface limits when the CG is in the most aft position.

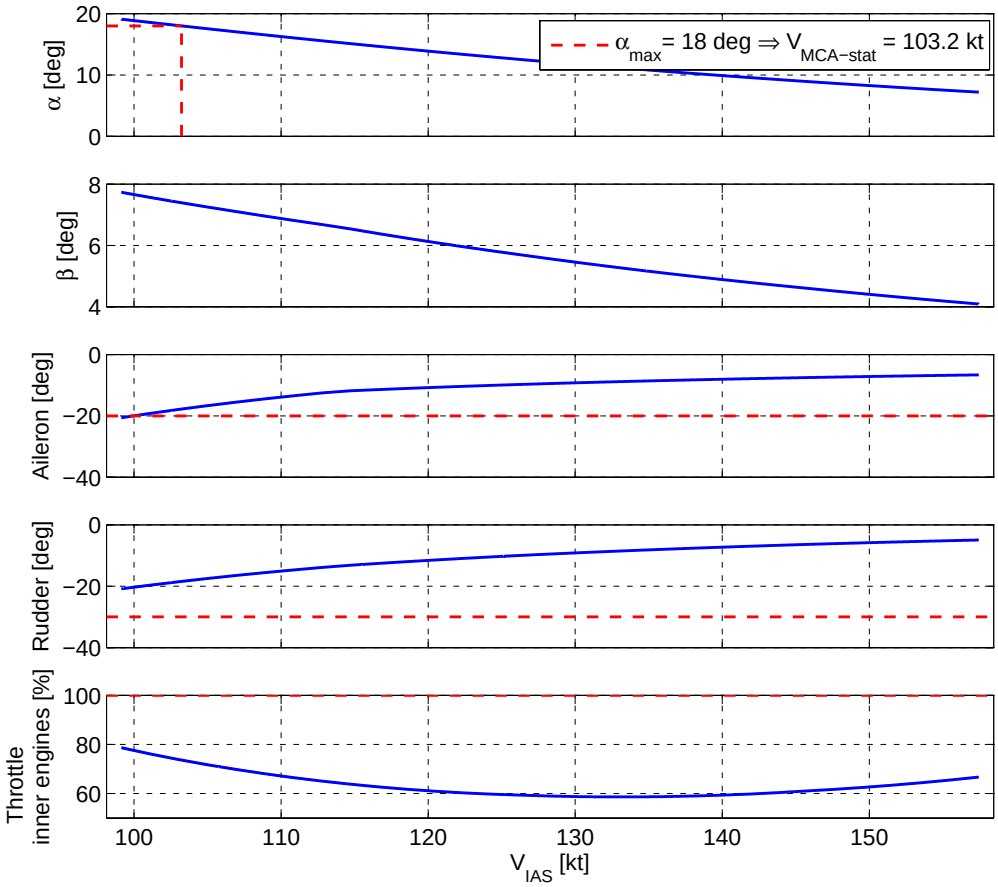

Figure 10. Determination of $V_{MCA-stat}$ for aircraft mass of 130 t and takeoff flaps setting (Static test)

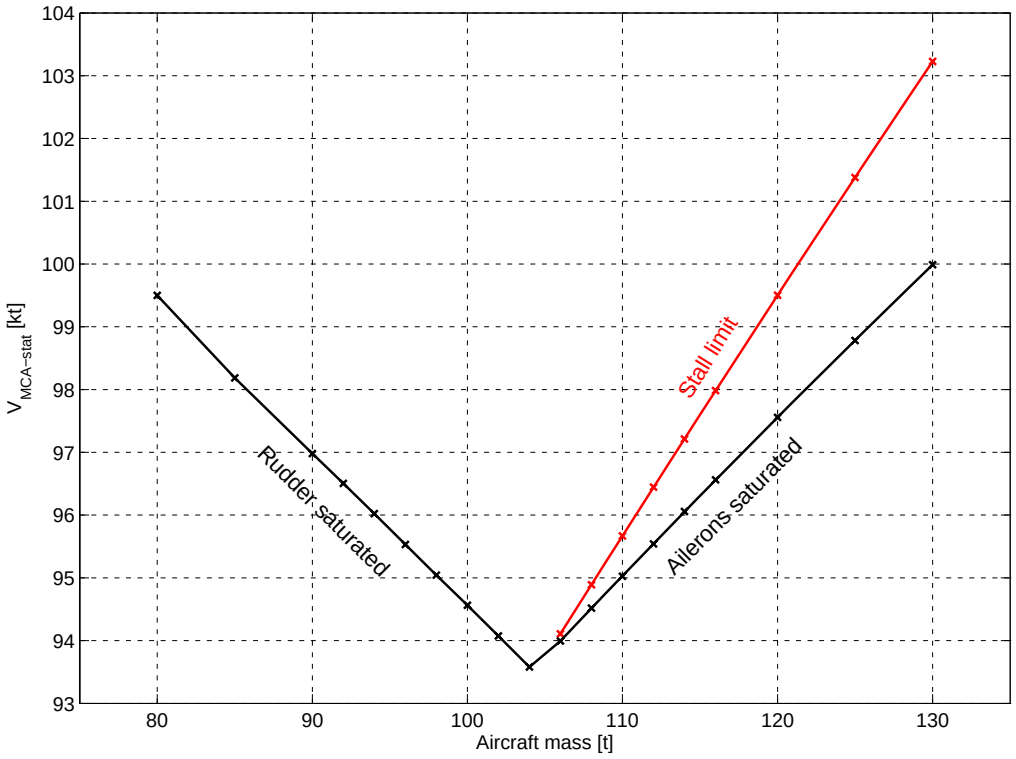

Figure 11. $V_{MCA-stat}$ depending on aircraft mass

Dynamic test

It must be proven by the V_{MCA} dynamic test that the aircraft can be controlled suffering an engine failure at V_{MCA}-static without special pilot training (see FAR 25). Airspeed has to be maintained and heading changes must not exceed 20°. If these conditions cannot be fulfilled V_{MCA} must be increased. In reality this test is performed through a series of flight tests in which one engine is switched off with decreasing speeds down to if possible V_{MCA}-static. For safety reasons these flight tests cannot be carried out close to the ground. The V_{MCA} determined in higher altitudes has to be adapted for the ground case. In the simulation, however, the engine failure can happen close to the ground directly after liftoff. The simulation test was automated as follows: The aircraft is trimmed for close to ground conditions, all engines at takeoff thrust and speeds down to V_{MCA}-static. After 0.5 s the left outer engine is switched off and controllers for rudder, aileron and elevator are used to stabilize the aircraft. The aim for the controllers is to set the heading Ψ back to the original value and to provide a pitch attitude for which steady climb is reached to continue the takeoff procedure.

The time histories of the most relevant flight parameters are shown in an example of such test in Figure 12. The aircraft was trimmed at an airspeed of 114 kt and takeoff thrust. For this condition a steady climb adjusts itself at an angle of attack α of 14° and a pitch angle Θ of 22 °. The control surfaces are not deflected (0°) and the trimming position of the horizontal stabilizer is about -9°. The red dashed lines in some time histories show the limits of the respective parameters. The red dots indicate the time of the left outer engine failure. The center of gravity of the aircraft is about 30 ft above the ground (see altitude plot). So the engine failure occurs directly after taking off (height at V_{LOF} is about 17 ft / see Fig. 4(a)). Because of the thrust asymmetry a positive angle of sideslip β and a negative change in flight direction Ψ is produced immediately. The corresponding yaw-roll moment generates a negative roll angle Φ. The pitch angle Θ decreases. Due to the flight direction change the controllers start to deflect the rudder and aileron up to their maximum negative deflection. Stabilization of the pitch attitude is accomplished by a controller for the elevator. Up to about 10 s after engine failure the rudder and ailerons stay fully deflected to reduce the deviation from

nominal flight direction. A quite big positive roll angle of about 35° is produced. The altitude at that time is sufficient to prevent ground contact of the wing tip. The angle of attack only increases marginally so that the distance to the stall limit is always adequate. The height loss after about 17 s leads to a minimum flight altitude of about 50 ft which is uncritical. After 35 s a widely stable steady climb into the direction of the original heading is achieved at a pitch angle of 17°, an angle of sideslip of 7° and a roll angle of 5°. Rudder and aileron deflection are about -14°, the elevator deflection is -4°.

The maneuver carried out in the test presented here to determine V_{MCA}-dynamic fulfills the above mentioned FAR 25 requirements. The aircraft could be stabilized after engine failure and the heading deviation stays within the required limits. The speed could be kept nearly constant. Indeed, the initial trimmed speed is 11 kt above V_{MCA}-static determined in the previous paragraph (see Fig. 10). However, the V_{MCA}-static of 114 kt is the lowest speed for the dynamic test at which the FAR 25 requirements can be still fulfilled. For lower speeds the angle of attack exceeds the stall limit, the heading deviation is exceeded or the aircraft touches the ground. Thus, $V_{MCA} = 114$ kt is fixed as the total result from both tests.

How a real even skilled pilot can perform this demanding maneuver without special training was not investigated further. Simulator trials will be carried out in future to develop and implement controller adaptations to a real pilot behavior.

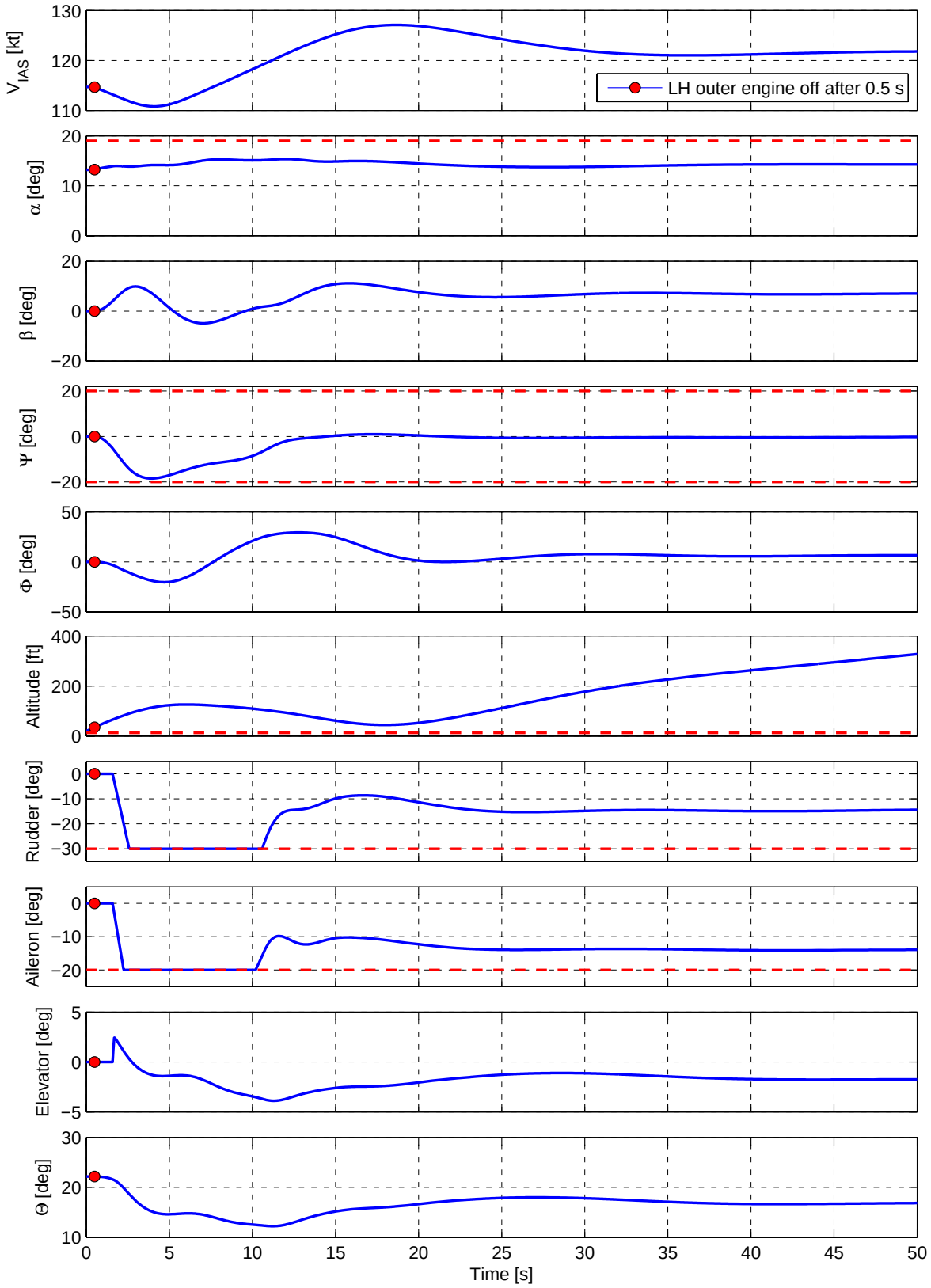

Figure 12. 'Engine out' test to determine $V_{MCA-dyn}$

IV. Landing Performance

For certification according to FAR 25 the required landing distance of an aircraft has to be proven. The landing distance is divided into two parts (see Fig. 2). The first segment (flight phase) begins when the landing gear crosses the 50 ft obstacle height and ends at touch-down of the main landing gear on the runway. Here the second part (ground phase) begins ending at the standstill position of the aircraft. The rotation phase from touch-down of the main landing gear to the touch-down of the nose wheel can be regarded as a part of the ground phase.

For an efficient determination of the landing distances from simulation a controller for automatic landing was implemented. Again, the behavior of human pilots might deviate from the controllers response. But for objective, repeatable investigations of flight physics the variation of individual pilot behavior should not be considered. The autoland controller consists of two subsystems for thrust and elevator control. A target flight path angle is calculated prior to the landing simulation and is stored in a lookup-table and is used as reference for flight path control. The autoland system is designed to minimize the deviation between reference and actual flight path angle. Shortly before the touch-down of the main landing gear at the end of the flare the thrust is switched to 'idle' position. After touch-down of the nose gear at the end of the rotation phase the braking is initiated. The spoilers are deflected fully, the landing gear brakes and the reverse thrust are initiated.

Figure 13 shows some parameters of an automatic landing versus the covered distance. The aircraft mass is 90 t at an approach speed of 97 kt and typical landing flaps position of 47°. The red dots indicate the touchdown of the main landing gear on the runway, the green dots denote the touchdown of the nose gear. The two upper diagrams of Figure 13 show the altitude and the flight path angle. The red dashed lines display the precalculated target values, the black curves illustrate the values flown in the simulation. The matching is quite good and the implemented controllers have adequate performance to fulfill their task. The approach flight path angle was set to -2.5°. At a distance of about 2900 ft and at an altitude of 65 ft the flare begins with a linear reduction of the flight path angle to -1 °. When reaching -1° the main landing gear touches the ground and initiates the landing shock recognizable in the sudden decrease of flight path angle or vertical speed (diagram below) down to zero. The vertical speed at touch-down is only 2.5 ft/s representing a very smooth landing. During the de-rotation phase the main landing gear shock strut compression can be recognized in the jagged patterns of vertical speed and flight path angle until touch-down of the nose gear. Then the braking is initiated to decelerate the aircraft to standstill position. The pitch angle diagram shows for the flight path angle of -2.5° a pitch attitude of 1.8° at the beginning of the landing phase. With the presumption of calm air this results into a low angle of attack of 4.3°. This allows the conclusion that the approach speed of 97 kt of this example is a high speed for the chosen FMTA aircraft configuration. During the flare the aircraft raises the nose until touchdown at theta of 5° and $\alpha = 6°$. After the subsequent de-rotation the nose wheel touches down at zero aircraft attitude and the nose gear's springy compression can be observed. During the braking process the aircraft remains at a small negative pitch attitude.

Figure 14 shows automatic landings, as explained before, for 5 different basic conditions. Each diagram shows the flight altitude of the aircraft center of gravity versus the covered distance for the last part of the landing. The red dashed lines mark the altitude at which the main landing gear crosses the 50 ft obstacle height (see Fig. 2). From here to standstill of the aircraft the landing distance is defined according to FAR 25 which is specified by the blue arrows and the indication 'Landing Distance'. The ground phase from touchdown of the main landing gear to standstill is specified by the blue arrows and the indication 'Ground phase'. The uppermost diagram shows the landing distances of the landing case explained in Figure 13. The second diagram shows the landing at the same aircraft mass, but for minimum landing speed of 68 kt. In this case the pitch angle Θ is a little less than 15° at touchdown what corresponds to the geometrical limit for runway touching of the aircraft tail. Due to the lower speed at touchdown the braking distance is shorter and so the total landing distance is reduced by around 483 ft. Nevertheless, the covered distance during the transition phase from touchdown of the main landing gear to the touchdown of the nose gear is longer. In contrast to 5° pitch attitude of the previous landing situation (see Θ diagram in Fig. 13) now a pitch attitude of 15° must be reduced to zero. The third diagram demonstrates the landing with the same aircraft mass and approach speed of the first case, but for a runway elevation of 8000 ft. Because of the lower aerodynamic drag as well as less efficient spoilers and thrust reverse the landing distance is extended

by an increment of about 366 ft. The fourth diagram shows the same landing under the condition of the first case but without thrust reverse and spoilers. As a consequence the landing distance is increased by about 144 ft. The last diagram of Figure 14 shows the most extreme case. Here the aircraft mass and landing speed are again as in the first case but the gear brakes have failed. The deceleration is effected only by thrust reverse and spoilers. This extends the landing distance by an increment of about 1855 ft to 4826 ft.

The 5 landing scenarios discussed above make clear which manifold possibilities are offered for the determination of the landing performance using the presented MAPET II tool. A landing distance determination with failures of thrust reverse, spoilers or gear braking might be difficult or for safety reasons even excluded from real flight testing.

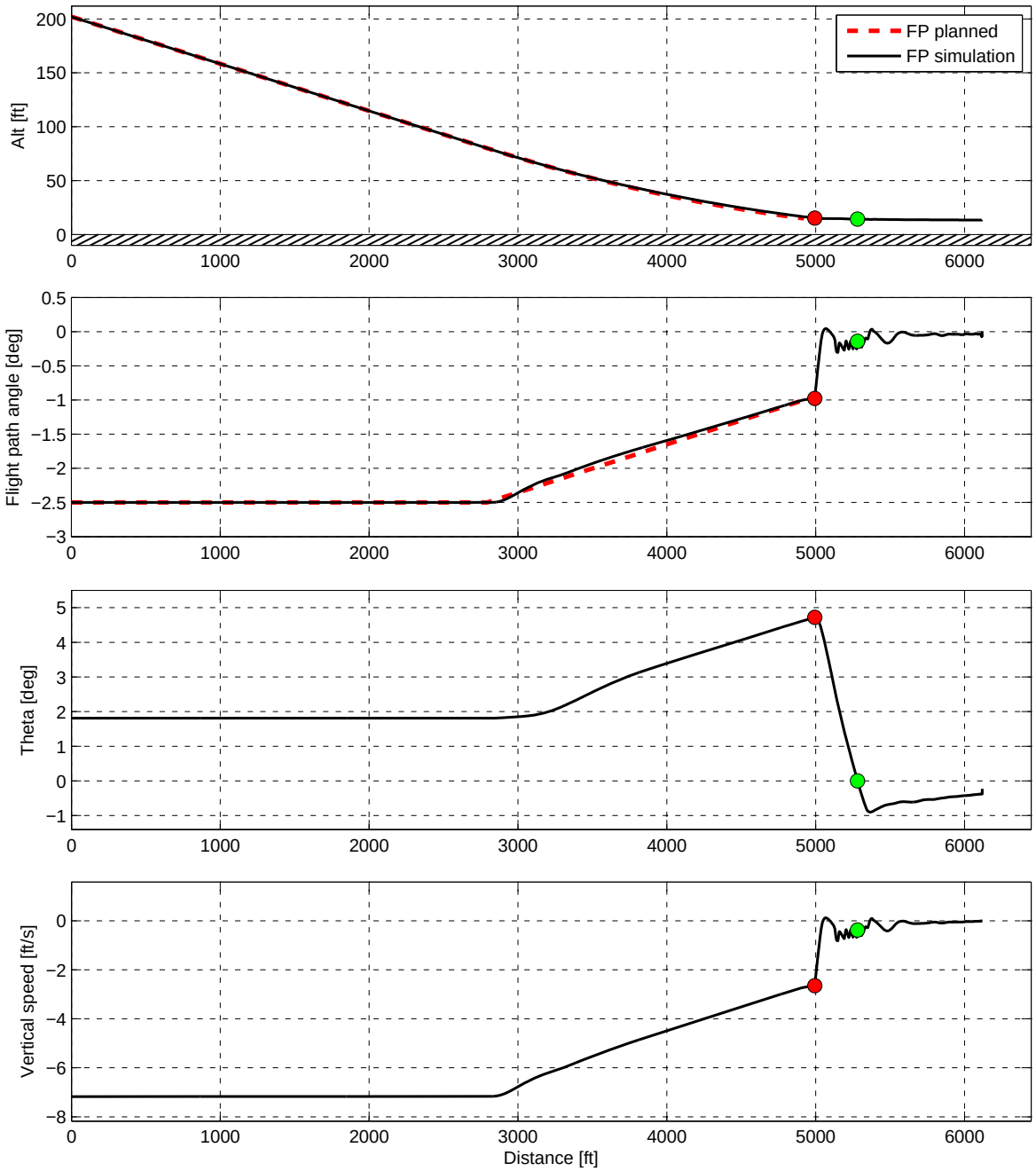

Figure 13. Altitude, flight path angle, pitch angle and vertical speed for automatic landing

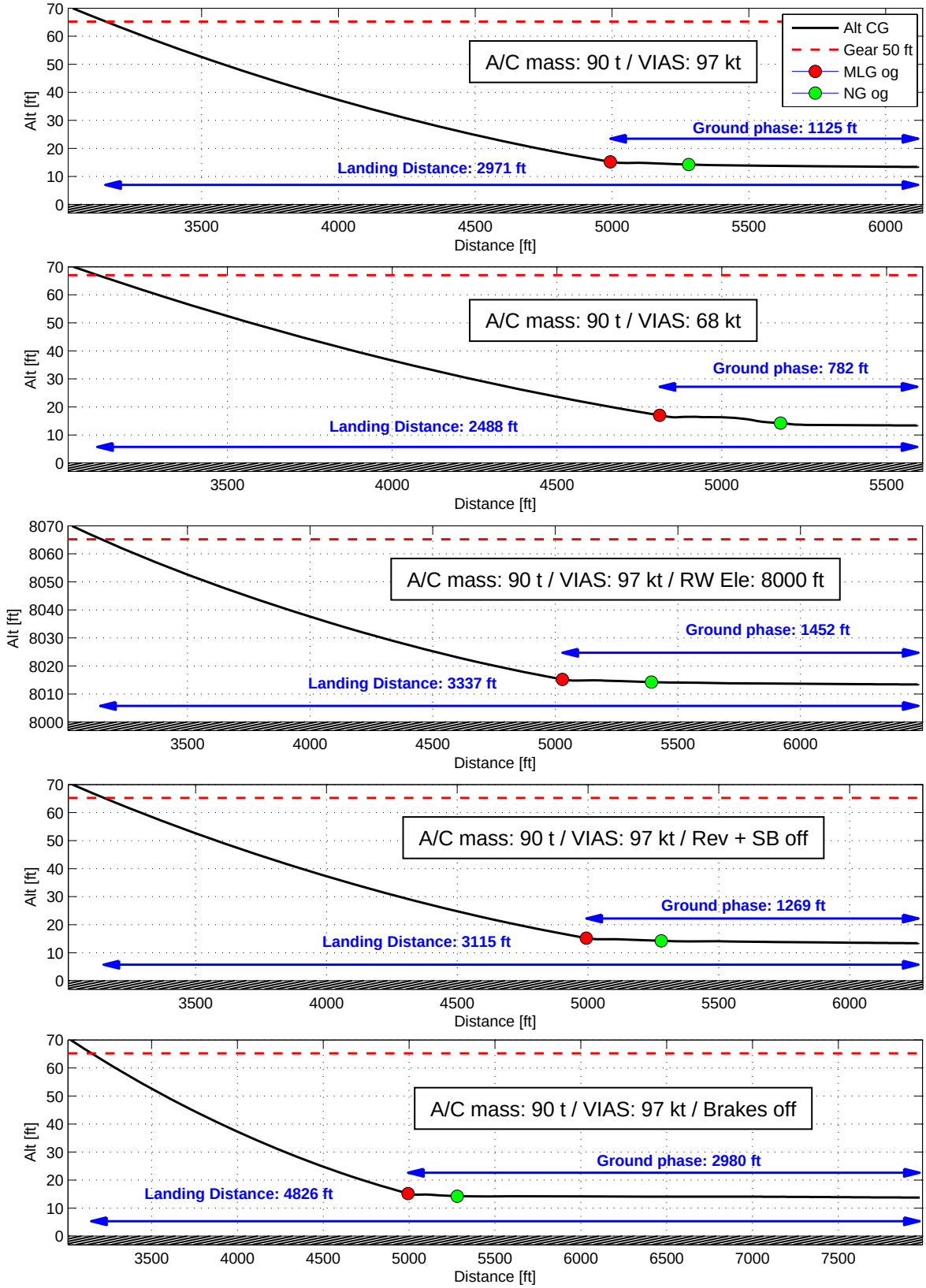

Figure 14. Landing distances for different conditions

V. Conclusion

This paper describes a model-based takeoff and landing performance evaluation by the new developed software tool MAPET II. The discussed results shown here refer exclusively to the flight-mechanical simulation model of the FMTA. Nevertheless, MAPET II is designed to provide the possibility of implementation of other models with similar structures. The takeoff performance is defined by reference speeds and covered distances during the takeoff phase (FAR 25). For MAPET II test scenarios for simulations were developed to determine these speeds according to the FAR instructions (Advisory Circular[4]). To allow an automated processing of the takeoff tests the pilot commands were substituted using controllers and switches with logical linkages. The execution and analysis of the different tests as well as the definition of important parameters like aircraft mass, CG position, flap setting or runway elevation are controlled via a central graphical user interface. Another feature of MAPET II is the determination of landing distances defined in the FAR 25. To perform automatic landings controllers were designed and implemented. Again a graphical user interface is used for the definition of main parameters of the landing condition like aircraft mass, approach speed and elevation and condition of the runway. Moreover, effects of failure cases like a loss of reverse thrust or spoilers can easily be analyzed.

The biggest advantages of the model-based determination of takeoff and landing performance are quickness, low costs and high flexibility. Depending on the computer power MAPET II allows to determine the takeoff reference speeds and the landing distances defined in FAR 25 within minutes for the integrated aircraft model. Of course, the quality of the so obtained data depends directly on the model fidelity. With high-quality models created by analytic methods, wind tunnel tests and CFD calculations which are normally provided before first flight an exact analysis of the takeoff and landing performance can take place using MAPET II. If a system identification using first flight test data is carried out later and thus a very exact adaptation of the model to the real aircraft behavior is achieved, the quality of the flight performance data can be increased. This precalculated data base can be used to plan flight test programs for determination of takeoff and landing performance more thoroughly so that maybe flight hours can be saved. A great advantage compared to real flight test performance evaluation gives the possibility to analyze the effects of failure cases or even configuration changes. Therefore the possibility to integrate any flight-mechanical simulation model (FMTA similar model structure), MAPET II can already be used in the aircraft design phase to make sure, that FAR requirements concerning takeoff and landing are fulfilled.

It should be noted that some uncertainty still exists for the settings of the used controllers and logically linked switches (brake initiation, engine out, etc.). Main focus of the work presented here was to study the compliance with FAR requirements by fulfilling the test scenarios in the most efficient way. But the design of controllers which show human pilot like control behavior was not subject of this study. As a consequence deviations have to be accepted between the data generated by MAPET II and data coming from real flight tests. Future work using simulator studies is planned on the adaptation of the controller settings and implementation of pilot models. Another option for the verification of MAPET II is based on the integration of a high fidelity model of an aircraft which is still in operation (e.g. VFW 614/ATTAS, C160 Transall) to compare the results with data from the aircraft operators manual.

References

[1]Ohme, P. and Raab, C., *A Model-Based Approach to Aircraft Performance Assessment*, AIAA Paper 2008-6873, Aug. 2008.

[2]Raab, C., *Flugmechanisches Gesamtmodell für ein zukünftiges Militärtransportflugzeug Version 1.0*, DLR - Institut für Flugsystemtechnik - IB 111-2007/05, May 2007.

[3]Lan, E., Roskam, J., *Airplane Aerodynamics and Performance*, DARcorporation, Lawrence, Kansas, USA, 2003.

[4]U.S. Department of Transportation, Federal Aviation Administration Advisory Circular, *Flight Test Guide for Certification of Transport Category Airplanes*, AC 25-7A, 3/31/98.

[5]FAA, *Pilot's Handbook of Aeronautical Knowledge*, FAA-H-8083-25A, 2008.

[6]Airbus Customer Service, *Getting to grips with aircraft performance*, January 2002.

[7]Thorbeck, J., *Manuskript zur Lehrveranstaltung Flugzeugentwurf, Teil H: Start und Landung*, Institut für Luft- und Raumfahrt, TU-Berlin, 2003.